https://doi.org/10.2352/ISSN.2470-1173.2018.11.IMSE-422


# Partial reset HDR image sensor with improved fixed pattern noise performance

***Volodymyr Seliuchenko, Vrije Universiteit Brussel (VUB), Brussel, Belgium, Melexis Inc., Nashua NH, USA, Sharath Patil, Marcelo Mizuki and Saad Ahmad, Melexis Inc., Nashua NH, USA, Maarten Kuijk, Vrije Universiteit Brussel (VUB), Brussel, Belgium***

## Abstract

*An efficient method is presented to achieve 4T pixel dynamic range extension whilst keeping the fixed pattern noise (FPN) low. The method utilizes the floating diffusion node as a secondary photocharge integration node with a partial reset applied to the floating diffusion node. The output image signal is a recombination of the linear signal integrated in the photodiode node, and a compressed signal integrated in the floating diffusion node. The recombination algorithm suppresses the FPN stemming from the variable transfer gate potential barrier height. An image sensor array of 1344x1008 pixels was built in 0.11um technology. We demonstrate the preservation of low light sensitivity of 4T pixels, a dark noise of 3.5e-, and a dynamic range for the current sensor of 115 dB, with potential to greatly exceed 120-dB. Further, the FPN stemming from the transfer gate potential barrier height variation does not degrade the image; the pixel compressive response can be controlled on a per frame basis depending on the scene, and the HDR scene is captured during one frame. The sensor combines the properties that are crucial for automotive and other machine vision applications.*

## Introduction

With reduction in pixel size driven by cost and camera size constraints, the achieved dynamic range gets smaller due to the reduction of the pixel's full well capacity. The typical dynamic range of linear image sensor pixels is below 80 dB, which is rather low compared to the dynamic range of the scenes that can occur in automotive or surveillance applications. For example, the dynamic range in night scenes with artificial illumination where the luminance can range from 0.1 $\frac{cd}{m^2}$ to 100 000 $\frac{cd}{m^2}$ can exceed 120dB ([1]). Other examples of high dynamic range scenes include a car entering or exiting a tunnel or a garage.

Many approaches were proposed to extend the dynamic range of image sensors [2]. Some dynamic range extension approaches, discussed below, are highly compatible with the mainstream linear CMOS pixel technology. That allows implementation of miniature high dynamic range (HDR) image sensors at the cutting edge of the pixel downscaling trend.

The simplest common method for HDR image acquisition comprises combining several images taken in a linear mode at different exposure times. This approach requires little or no changes to the typical image sensor architectures and works very well for static or slow changing scenes. However, for scenes requiring high frame rates, such as automotive scenes, ghosting artifacts may appear because the images with different exposures are taken at different times [3]. Practically, about 2 or 3 frames are used for HDR image fusion, leading to a possible detail loss in the reconstructed HDR image at the transition between exposures [4, 5]. Also, the multiple acquisition HDR approach has a reduced dark performance due to gaps in the signal integration which occur during a readout of low exposure frames. The ghosting artifacts can be reduced by lowering the time gap between image acquisitions using an additional in-pixel memory [6, 7], however, such in-pixel memory is also practically limited to 2 or 3 frames due to pixel fill factor constraints.

Another example of an image sensor dynamic range extension approach, highly compatible with the mainstream linear image sensor technology, comprises a mosaic of neutral density filters placed on top of the pixel array [8]. It allows extension of the dynamic range but sacrifices dark performance and lateral resolution.

Logarithmic sensors exploit a non-linear element connected to the photocharge integrating node which defines the pixel compressive response. These sensors can achieve dark sensitivity similar to linear image sensors since they acquire the whole HDR image during a single frame. However they suffer from increased fixed pattern noise (FPN) in the logarithmic region and may require extensive calibration [9, 10, 11, 12].

The method of image sensor dynamic range extension, described in the work of S. Decker et al [13], exploits partial reseting of the 3T pixel sense node during the integration time. The reset gate timing defines the pixel response function which can be tuned to match the scene preserving image details over a wide range of optical powers [5]. Dark sensitivity of the 3T pixels is not deteriorated since the HDR image is captured within one frame, there are no large gaps in the integration of the photo signal that happen e.g. when the HDR image is obtained from multiple exposure frames. Also, since no additional elements are added to the 3T pixel, the pixel fill factor is not reduced comparing to the linear pixel. Therefore, this approach could be well suited for applications like automotive that require an extended dynamic range, a high sensitivity and a high framerate. However, the range extension concept described in [13] requires using a 3T pixel which has inferior noise performance comparing to 4T pixels. Application of this method to the most sensitive and widely used 4T pixels is not straightforward but can be done as explained in the next sections.

## Partial reset dynamic range extension applied to 4T pixels

Figure 1 (a) shows a 4T pixel cross section and the corresponding potential diagram with a partial reset applied to the photo charge integrating node *PD* using the transfer gate *TX* in a similar way as described in [13]. During the exposure time the reset gate potential *RT* is kept high so that the charge, overflowing the transfer gate during the partial reset *TX*, is discarded into

the supply terminal $Vdd$. At the end of exposure time the signal from the $PD$ node is read out using a conventional 4T pixel readout method. This mode of operation allows for extension of the dynamic range providing a flexible control of the pixel transfer function as in [13]. The temporal noise performance of a 4T pixel is preserved, however, the image fixed pattern noise turns out to be significantly higher than typical FPN of image sensors based on 3T pixels used in [13].

For the purpose of FPN comparison, the same 4T pixel was configured in a 3T mode of operation as shown in Figure 1 (b): the transfer gate $TX$ potential was constantly set high and the reset gate $RT$ was used to apply the partial reset to the photo charge integrating node $FD$ in a similar way as described in [13]. At the end of exposure time, the signal is readout as a difference between the voltage integrated in the $FD$ node and the reset voltage of the $FD$ node $\phi_{R\,FD}$. In this mode of operation, the reset temporal noise is not cancelled by the conventional 4T pixel readout scheme.

The FPN comparison experiment was set up with the image sensor illuminated using a uniform light source strong enough to saturate the integrating potential wells with photo charge. Before the readout, a partial reset using the transfer gate $TX$ was applied to the integrating node $PD$ for the mode of operation illustrated by Figure 1 (a) and a partial reset using the reset gate $RT$ was applied to the integrating node $FD$ for the mode of operation illustrated by Figure 1 (b). A series of frames were captured for both modes of operation. FPN was estimated by calculating a standard deviation over the averaged series of captured frames. For the 4T mode of operation (Figure 1 (a)), the measured FPN peaks at 6% of the full signal swing, while the measured FPN for the 3T mode of operation (Figure 1 (b)) is below 1% of the full signal swing. The increased FPN of the 4T mode can be explained by the pixel to pixel variation of the partial reset potential barrier $b_{PR\,TX}$ which is defined by the difference of the uncorrelated reset potential $\phi_{R\,PD}$ and partial reset potential $\phi_{PR\,TX}$. In contrast, in the 3T mode shown in Figure 1 (b), the partial reset barrier $b_{PR\,RT}$ is defined by the reset potential $\phi_{R\,FD}$ and partial reset potential $\phi_{PR\,RT}$ which are highly correlated since they both are set by the same gate $RT$. Thus, the pixel to pixel variation of the partial reset potential barrier $b_{PR\,RT}$ is much less compared to the variation of $b_{PR\,TX}$.

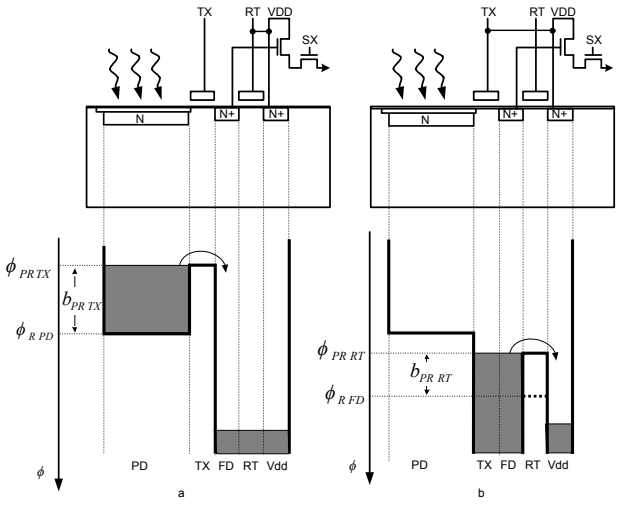


***Figure 1.*** *Barrier height measurement: transfer gate (a) and reset gate (b)*

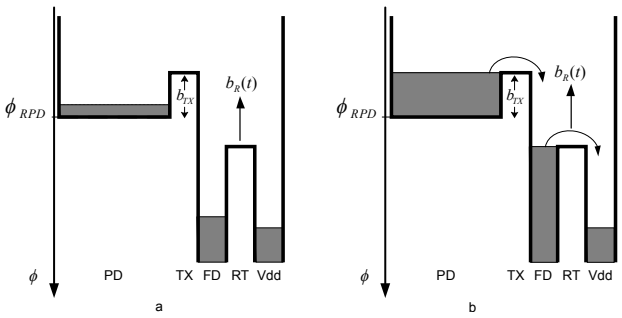


***Figure 2.*** *4T pixel potential diagram operating in proposed HDR mode*

In this work, we propose a method of dynamic range extension that preserves the dark temporal noise performance of 4T pixels while supressing the FPN stemming from the technological variation of the transfer gate $TX$ potential barrier and photodiode reset potential.

## FPN reduction method

The proposed method utilizes the floating diffusion node $FD$ as a secondary integrating node. The signal is split into two parts by lowering the transfer gate $TX$ potential barrier so that during the exposure the charge can overflow from the photodiode potential well $PD$ to the floating diffusion potential well $FD$ once the photodiode potential well $PD$ gets full. The reset gate $RT$ is used to apply partial resets to the floating diffusion node $FD$. The signal split level, at which the overflow occurs, is not well defined due to the technological variation, thus both $PD$ and $FD$ signals contain a high amount of FPN. However, the total amount of charge, integrated in both $PD$ and $FD$ nodes is independent of this split level, and is, thus, free of FPN stemming from the technological variation of the transfer gate $TX$ potential barrier and photodiode reset potential $\phi_{R\,PD}$. This concept is utilized in the proposed FPN reduction method.

The potential diagram shown in Figure 2 illustrates the proposed method of 4T pixel dynamic range extension under two illumination conditions. In the low light conditions (Figure 2, (a)), the pixel operation is not very different from the operation of a linear sensor: the photo charge is integrated in the photodiode potential well $PD$ and, at the end of integration, this photo charge is transferred to the floating diffusion $FD$ for readout. Under high light conditions (Figure 2, (b)), the photodiode potential well $PD$ gets filled and the photo charge overflows to the floating diffusion $FD$ where the integration continues in a non-linear way due to partial resets $b_R(t)$ being applied to the floating diffusion node $FD$ using the reset gate $RT$. At the end of the integration time , the pixel's select gate SX is activated and signal readout is done in three steps: first the voltage of the floating diffusion $V_{\mathrm{FD}}$ is sampled, then, the floating diffusion node $FD$ is reset by activating the reset gate $RT$ and the pixel reset voltage $V_R$ is sampled, and, finally, the transfer gate $TX$ is activated transferring all the charge from the photodiode node $PD$ to the floating diffusion $FD$ and the third sample of the pixel's output $V_{\mathrm{PD}}$ is acquired. The last two steps of the readout constitute a typical correlated double sam-

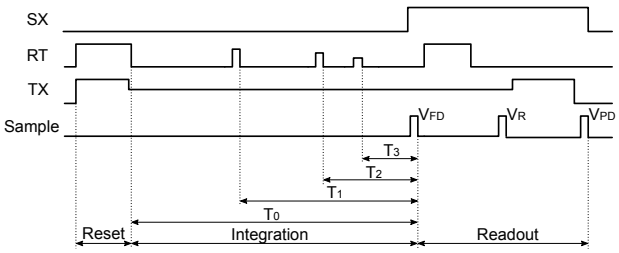


***Figure 3.*** *Timing diagram*

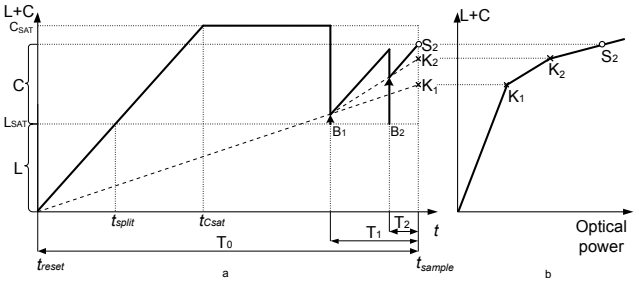


***Figure 4.*** *Signal integration (a) and pixel response (b)*

pled readout of a linear sensor – the linear signal $L$ is calculated as a difference between the reset voltage $V_R$ and the last sample $V_{\mathrm{PD}}$. The nonlinear compressed signal $C$ is derived as a difference between the reset voltage $V_R$ and the first sample $V_{\mathrm{FD}}$:

$$L = V_R - V_{\mathrm{PD}}, \qquad C = V_R - V_{\mathrm{FD}} \tag{1}$$

Figure 3 shows a complete timing diagram of the 4T pixel operating in the proposed HDR mode which can be logically divided into reset, integration and readout phases. The operation starts with a reset of the floating diffusion $FD$ and the photodiode $PD$: all the charge is cleared from the photodiode potential well and the floating diffusion potential is set to the supply potential minus a reset gate threshold voltage. At the end of the reset phase the voltage of the reset gate $RT$ is set to ground, and the transfer gate $TX$ is biased to some intermediate voltage, chosen such so that the linear signal $L$ saturates slightly below the saturation of the signal chain.

The high dynamic range signal $S_{\mathrm{out}}$ is derived from the linear signal $L$ and the compressed signal $C$ as shown in equation (2). For low optical power, when the linear signal $L$ is below saturation, the linear signal $L$ propagates to the output $S_{\mathrm{out}}$ unchanged, and the compressed signal $C$ is ignored. Once the linear signal $L$ approaches saturation, it gets summed with a linearized compressed signal $C$ – this sum represents the total photo charge detected by the pixel and thus it does not contain FPN of the transfer gate potential barrier. Since the floating diffusion is slightly light sensitive, an additional attenuation $\alpha$ is applied. Finally, the signal gets compressed ($f_R$) to fit the bus bit width of the output interface.

$$S_{\mathrm{out}} = \begin{cases} f_R\left(L + \alpha \cdot f^{-1}(C)\right), & \text{if } L > L_{\mathrm{TH}} \\ L, & \text{if } L \le L_{\mathrm{TH}} \end{cases} \tag{2}$$

where $f^{-1}$ is the inverse function to the compression function $f$ which is defined by the partial reset barrier function $b_{\mathrm{R}}(t)$, $L_{\mathrm{TH}}$ is a threshold value which is selected to be slightly below the point where the linear signal saturates, and $f_R$ is the recompression function used fit the HDR signal into the limited bit width of the output interface. In a general case, $f_R$ can be different from $f$.

Since the signal is integrated in two separate nodes, the analytical expression for the compression function $f$ is different from [5] and [13]. Figure 4 (a) shows photocurrent integration process of the 4T pixel operating in the proposed mode for two partial reset pulses applied, and Figure 4 (b) shows a corresponding pixel response with two knee points. For illustration purposes, it is best to analyze the $L+C$ signal – the compressed signal $C$ can be put on top of the linear signal $L$. The solid line in Figure 4 (a) represents a signal high enough to be affected by the second partial reset. Integration starts at time $t_{\mathrm{reset}}$ with both $L$ and $C$ initialized to zero. Once the linear signal saturates at time $t_{\mathrm{split}}$, the signal overflows from the photodiode to the floating diffusion where the photocurrent integration continues. The compressed signal saturates at time $t_{\mathrm{Csat}}$ where it stays saturated until the first partial reset occurs at time $t_{\mathrm{reset}} + (T_0 - T_1)$. The partial reset pulse applied to the reset gate lowers the potential barrier adjacent to the floating diffusion so that a signal above a certain level ($B_1$, $B_2$ … $B_n$) leaks to the supply utill it reaches this level, and the signal below this level ($B_1$, $B_2$ … $B_n$) remains unaffected. After integration time $T_0$ the signals $L$ and $C$ are sampled at time $t_{\mathrm{sample}}$. The levels $B_1, B_2 \ldots B_n$ will be further referred to as partial reset heights; in practice, their values can be measured by placing a partial reset at a time very close to the readout time $t_{\mathrm{sample}}$.

The knee point position is determined by the partial reset heights and partial reset barrier timings:

$$K_i = \frac{T_{i-1}}{T_i - T_{i-1}}\left(B_{i-1} - B_i\right) + B_{i-1}, \quad for\ i \ge 2 \tag{3}$$

Formula (3) is valid only for the second or further kneepoints for which the partial reset potential barrier heights are defined with respect to the floating diffusion reset voltage. The first kneepoint is an exception because its knee point position is also determined by the linear signal saturation:

$$K_1 = \frac{L + B_1}{T_0 - T_1} \cdot T_0 - L \tag{4}$$

At each knee point the slope of the pixel's response function changes by the ratio $\mathrm{SR}_i$ of the effective integration times for the segment before the knee point and the segment after the knee point:

$$\mathrm{SR}_i = \frac{T_{i-1}}{T_i}, \quad for\ i \ge 1 \tag{5}$$

$SR_i$ and $K_i$ are the required parameters for the linearization, the high dynamic range signal $H$ can be calculated using the formula:

$$H = L + \sum_{i=0}^{N}\left(\left(K_i - K_{i-1}\right) \cdot \prod_{j=0}^{i} SR_{j-1}\right) + \left(C - K_N\right) \cdot \prod_{j=0}^{N} SR_j\ , \tag{6}$$

where $N$ is the index of the highest knee point which is below signal $C$, $K_{i<1} = 0$ and $SR_{i<1} = 1$.

The maximum achievable dynamic range is similar to the maximum achievable dynamic range of the 3T based image sensors [2]. The dynamic range extension factor can be approximately calculated as:

$$\mathrm{DR}F_{\max} \approx 20 \cdot \log \frac{C_{\mathrm{SAT}} - K_{\mathrm{ls}}}{C_{\mathrm{SAT}}} \cdot \frac{T_0}{T_{\mathrm{ls}}} \tag{7}$$

where $C_{\mathrm{SAT}}$ is a saturation level of the compressed signal, $K_{\mathrm{ls}}$ is the chosen position for the last knee point, $T_{\mathrm{ls}}$ is the chosen effective integration time for the last segment. For a practical case of 30 frames per second, $T_0 = 33ms$, $\frac{C_{\mathrm{SAT}} - K_{\max}}{C_{\mathrm{SAT}}} = \frac{1}{5}$, $T_{\mathrm{ls}} = 5us$ the dynamic range extension factor can be as high as $\mathrm{DR}F_{\max} \approx 62dB$.

## Experimental results

To test the proposed concept, an image sensor was designed in CMOS CIS 0.11um technology. It contains a 1344x1008 array of 4T pixels with 3.75um pixel pitch, 12 bit sigma-delta column ADCs, a programmable partial reset sequencer for the pixel response function definition, row SRAM for storing the $L$ and $C$ signals and digital logic circuits including a parallel video interface, a timing generator, an image processing pipeline and a microprocessor. The image processing pipeline contains dark current correction, defect pixel correction, image statistics collection, 2D filter cores, tone mapping blocks and DSP blocks for the HDR recombination algorithm. The microprocessor can run algorithms analyzing image statistics, automatically reconfiguring the image partial reset sequencer and the array timing generator in real time to achieve optimal exposure of the HDR scene fully exploiting the flexibility of the partial reset approach.

**Table 1 Summary of the image sensor performance**

| | |
|---|---|
| Technology | 0.11um |
| Resolution | 1344 x 1008 pixels |
| Chip size | 8.4 x 9 mm |
| Pixel size | 3.75 x 3.75 um |
| Maximum frame rate | 45 frames per second |
| Linear dynamic range | 67 dB |
| Dynamic range | 115 dB |
| Total dark noise | 3.5 $e^-$ |
| QE @ 535nm | 44% |
| Conversion gain | 71 uV/ $e^-$ |
| Power consumption | 0.6W |

Table 1 summarizes the sensor specifications. A low dark noise of 3.5 $e^-$ was achieved along with a maximum dynamic range of 115 dB. The achieved dynamic range extension factor is limited by the continuously sampling delta-sigma ADC which restricted the minimum possible partial reset time $T_{\mathrm{ls}}$ to about 25us. The floor plan of the sensor is shown in Figure 5.

Figure 6 shows a measured plot of average signal $S_{\mathrm{out}}$ and a measured plot of FPN for the linear signal $L$, the compressed signal $C$ and the output chip signal $S_{\mathrm{out}}$ as a function of the incident optical power. The dynamic range of this configuration is about 115dB. The plot can be subdivided into 3 segments:

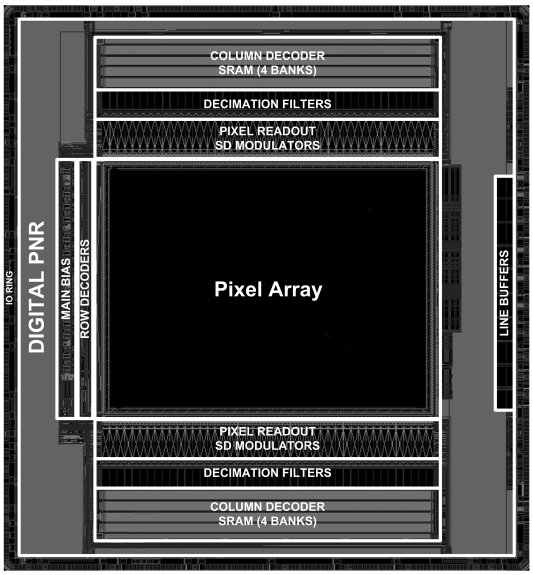


***Figure 5.*** *Image sensor floorplan*

- linear segment is below linear signal saturation, the pure linear signal is output with low FPN which has a typical increasing trend characterized by photo response non-uniformity (PRNU);
- recombination segment is above the linear saturation where the FPN of the linear and compressed signals spikes above 5%, however the output signal FPN is below 1%;
- compressed segment where FPN is below 1% and is mostly defined by the FPN of the reset gate.

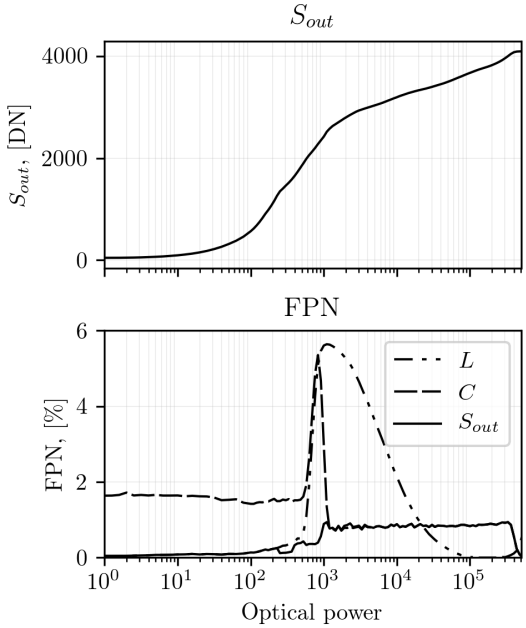


***Figure 6.*** *Measured FPN and $S_{out}$ versus optical power*

Figure 7 shows a comparison of images of a dark scene and a bright scene acquired using the image sensor operating in a linear mode (a, d), dynamic range extension mode with partial resets applied to the photodiode node (b, e, g) and the proposed method (c, f, h). The images of the dark and bright scenes were taken with exactly the same settings for each mode at the rate of 37 frames per second.

For a better comparison, a gamma correction of 0.45 was applied to the dark scene images (a, b, c) to make the dark details more visible. All three methods exhibit equal performance for the dark scenes, therefore, the low noise advantages of 4T pixel are preserved.

The luminance of the brightest patches in the bright scene was chosen to be $1.5 \cdot 10^5$ times higher than in the dark scene ($0.04\ \frac{cd}{m^2}$), thus, the scene dynamic range was higher than 100dB. The image (d), taken with an image sensor operating in linear mode, is mostly saturated, thus the major part of the image is in the non-linear region. The image (e) was acquired with a sensor operating in the photodiode partial reset mode and the image (f) was acquired with a sensor operating in the proposed mode. The dynamic range extension settings were chosen to be quite close for both methods as it can be seen from the images (e) and (f), however, the noise level in (e) is visibly higher. For a better comparison, the part of the images, designated with a dash-dot rectangle, is magnified and shown in (g) and (h). As expected, FPN of the image (h), acquired using the proposed method, is significantly smaller than FPN of the image (g) acquired with a sensor operating in a photodiode partial reset mode.

## Conclusion

The proposed method of 4T pixel dynamic range extension, utilizing the floating diffusion node as a secondary photo charge integration node with a partial reset applied to it, is highly effective at cancelling the transfer gate FPN. An image sensor array of 1344x1008 pixels built in 0.11um technology demonstrated the feasibility to combine the properties that are crucial for automotive and other machine vision applications: low light sensitivity preservation of 4T pixels, a dark noise of 3.5e-; a dynamic range for the current sensor of 115 dB, that has the potential to greatly exceed 120 dB.

## References


[1] Dirk W. Hertel and Edward Chang. Image quality standards in automotive vision applications. In *Intelligent Vehicles Symposium, 2007 IEEE*, pages 404–409. IEEE. 60.

[2] Arthur Spivak, Alexander Belenky, Alexander Fish, and Orly Yadid-Pecht. Wide-dynamic-range CMOS image sensors. comparative performance analysis. 56(11):2446–2461. 80.

[3] Takao Jinno and Masahiro Okuda. Multiple exposure fusion for high dynamic range image acquisition. 21(1):358–365.

[4] N. Barakat, T. E. Darcie, and A. N. Hone. The tradeoff between SNR and exposure-set size in HDR imaging. In *2008 15th IEEE International Conference on Image Processing*, pages 1848–1851.

[5] Dirk Hertel, Andrew Betts, Rich Hicks, and Machiel ten Brinke. An adaptive multiple-reset CMOS wide dynamic range imager for automotive vision applications. In *Intelligent vehicles symposium, 2008 IEEE*, pages 614–619. 90.

[6] N. Akahane, S. Sugawa, S. Adachi, K. Mori, T. Ishiuchi, and K. Mizobuchi. A sensitivity and linearity improvement of a 100-dB dynamic range CMOS image sensor using a lateral overflow integration capacitor. 41(4):851–858.

[7] C. Ma, Y. Liu, Y. Li, Q. Zhou, X. Wang, and Y. Chang. A 4-m pixel high dynamic range, low-noise CMOS image sensor with low-power counting ADC. 64(8):3199–3205.

[8] Saul D. Freedman and Farid Boussaid. A high dynamic range CMOS image sensor with a novel pixel-level logarithmic counter memory. In *Knowledge-Based Engineering and Innovation (KBEI), 2015 2nd International Conference on*, pages 14–19. IEEE.

[9] Bhaskar Choubey and Steve Collins. Models for pixels with wide-dynamic-range combined linear and logarithmic response. 7(7):1066–1072.

[10] D. Joseph and S. Collins. Modeling, calibration, and correction of nonlinear illumination-dependent fixed pattern noise in logarithmic CMOS image sensors. 51(5):996–1001.

[11] Spyros Kavadias, Bart Dierickx, Danny Scheffer, Andre Alaerts, Dirk Uwaerts, and Jan Bogaerts. A logarithmic response CMOS image sensor with on-chip calibration. 35(8):1146–1152.

[12] G. Storm, R. Henderson, J.E.D. Hurwitz, D. Renshaw, K. Findlater, and M. Purcell. Extended dynamic range from a combined linear-logarithmic CMOS image sensor. 41(9):2095–2106.

[13] Steven Decker, D. McGrath, Kevin Brehmer, and Charles G. Sodini. A 256x256 CMOS imaging array with wide dynamic range pixels and column-parallel digital output. 33(12):2081–2091.


## Author Biography

*Volodymyr Seliuchenko received BS and MS degrees from Zhytomyr Technological University in 2005. He is currently pursuing a PhD degree at the ETRO dept. of the Vrije Universiteit Brussel. His research interests comprise of 2D/3D image sensors and computer vision. In 2006, he joined Melexis where he is currently focusing on research and development of 2D and 3D image sensors.*

*Sharath Patil received a BE degree in Electronics and Communications from Visvesvaraya Technological University, India, in 2007 and the MSEE degree from University of Texas Arlington in 2011. He has been with Melexis since 2011 and is currently enrolled as a part-time student at University of Massachusetts, Lowell, USA pursuing his PhD degree in Electrical Engineering.*

*Marcelo Mizuki received a B.E.E. degree in electrical engineering from the Georgia Institute of Technology, Atlanta, GA, in 1994, and an MS degree in electrical engineering from the Massachusetts Institute of Technology (MIT) Cambridge, MA, USA, in 1997. In 2008, he joined Melexis Inc where he is currently System Architect. His areas of interest include imager sensors, time of flight and ranging and circuit and system design.*

*Saad Ahmad is a senior design engineer at Melexis and works on 2D/3D sensors. His design interests are in the field of switch-cap circuits and ADCs.*

*Maarten Kuijk is a professor of electrical engineering at the ETRO dept. of the VUB. His current research topics include electrical and optical interconnects devices & building blocks, optoelectronic devices & sensors, CMOS analog and digital circuits. He authored and co-authored more than 100 international refereed publications and over 20 international patents. He is founder of the VUB spin-off "EqcoLogic NV" that defined the physical layer of the international high-end camera interface-standard "CoaXPress". EqcoLogic was acquired by Microchip Technology in 2013. He also co-founded "SoftKinetic Sensors N.V" for Time-Of-Flight CMOS image sensors and cameras, which got acquired by Sony Corporation in 2015.*

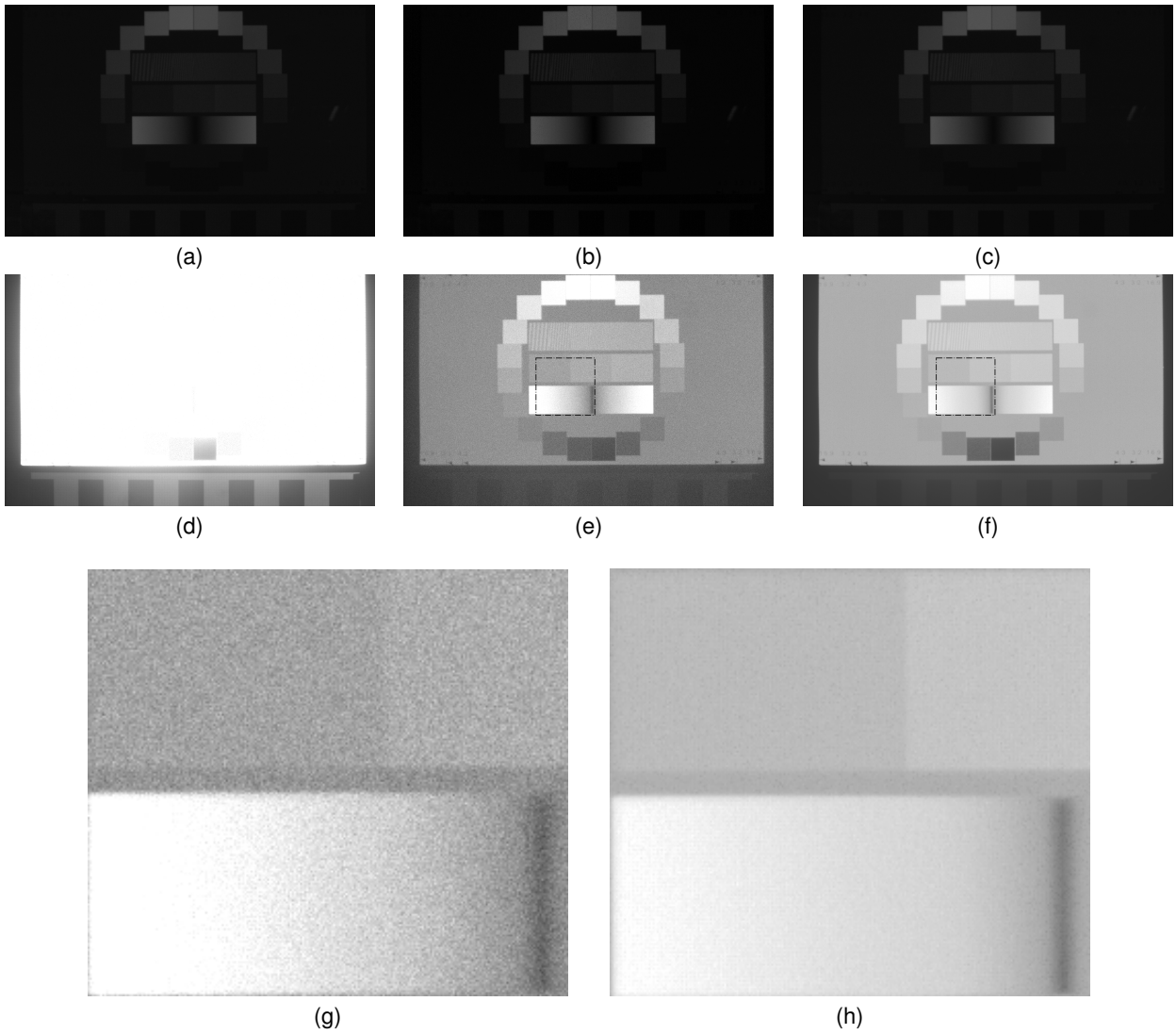


***Figure 7.*** *Comparison of the partial reset dynamic rage extension methods: a, d - linear mode, b, e, g - partial reset is applied to the photodiode, c, f, h - proposed method*